

How square ice helps lubrication

Astrid S. de Wijn^{1,2} and Lars G. M. Pettersson¹

¹*Department of Physics, Stockholm University, 10691 Stockholm, Sweden*

²*Department of Engineering Design and materials,
Norwegian University of Science and Technology, 7491 Trondheim, Norway*

In the context of friction we use atomistic molecular-dynamics simulations to investigate water confined between graphene sheets over a wide range of pressures. We find that thermal equilibration of the confined water is hindered at high pressures. We demonstrate that, under the right conditions, square ice can form in an asperity, and that it is similar to cubic ice VII and ice X. We simulate sliding of the square ice on atomically flat graphite and find extremely low friction due to structural superlubricity. The conditions needed for this equilibration correspond to low sliding speeds, and we suggest that the ice observed in experiments of friction on wet graphite is of this type.

PACS numbers:

I. INTRODUCTION

The combination of water with graphite or graphene is under active investigation in several fields for a number of reasons. In the field of tribology, it is of interest due to the action of graphite powder as a solid lubricant, which is far more effective under humid conditions than in vacuum or dry air. This is opposite to the case for other solid lubricants, such as WS_2 and MoS_2 ¹. Moreover, water alone is a poor lubricant, due to its low viscosity-pressure coefficient. While suggestions have been made as to the reason behind water's beneficial effects on graphite as a lubricant^{2,3}, this effect is not yet understood.

A number of high-profile experimental^{4–7} and numerical^{8–10} studies have investigated water confined using graphene or carbon nanotubes under various conditions. Under sufficiently strong confinement water doesn't crystallize and thus, by confining water inside, e.g., nanotubes or zeolite pores it is possible to investigate liquid water well below the temperature of homogeneous ice nucleation (for a recent review, see¹¹). These studies have found that when water is confined between graphene sheets or graphite, there is clear structure in the direction normal to the surfaces but the in-plane order is typically either liquid-like or hexagonal. In the case of the hexagonal structure there are, however, different opinions on whether or not it is related to the graphite structure^{8,10}. In simulations of water in carbon nanotubes¹², another structure was found where water arranges into a rolled-up square structure. Square ice has also been observed in experimental studies of water confined between graphene sheets⁴. Han et al.¹⁰ focused on the question whether a critical point could exist on the liquid-solid coexistence line and used the pressure dependence of water structure confined between two smooth hydrophobic plates to derive the phase diagram in this region. They find only a narrow coexistence region between the liquid and square ice solid without commenting on the structure of the square ice.

Different aspects on the role of water in lubrication have been reported^{3,13}. In their experiments Jinesh and Frenken found capillary condensation of water, which at

room temperature formed ice between the asperity and substrate, to lead to sticking rather than lubrication¹³. Similarly, Berman et al.³ found that in simulations water increased friction in their system where graphene flakes were combined with nanodiamonds. In the present work, in contrast, we find that water in between graphene sheets, and in the form of room temperature square ice, leads to superlubricity.

All of the numerical studies mentioned above that deal with the phase diagram of confined water are concerned with systems in equilibrium. However, a sliding contact produces local changes in pressure and temperature and is typically out of equilibrium. Moreover, the structure in a sliding contact can be of enormous influence on the friction. Mismatched lattice parameters, especially, can lead to extremely low friction, known as structural superlubricity (see, for example¹⁴).

Experiments measuring the friction of an AFM tip on graphite covered in water^{13,15} have indeed demonstrated interesting velocity dependence. At low sliding velocities, a stick-slip period of 3.8 Å was observed, which does not correspond to any period of graphite. At higher sliding speeds, the normal graphite period was present instead. This behaviour was also found to be related to air humidity. This implies that under at least some sliding conditions, ice can be formed on a graphite substrate at room temperature.

In this work, we use MD simulations to study the combination of water and graphite in the context of friction and out-of-equilibrium dynamics. As the pressure in a single asperity can be up to several tens of GPa, we pay particular attention to high pressures. We find that thermal equilibration of the confined water is hindered at high pressures. We demonstrate that, under the right conditions, square ice can form, and that it is similar to cubic ice VII and ice X. The conditions needed for this equilibration correspond to low sliding speeds, and therefore suggest that the ice observed in the friction experiments^{13,15}, is cubic VII or X.

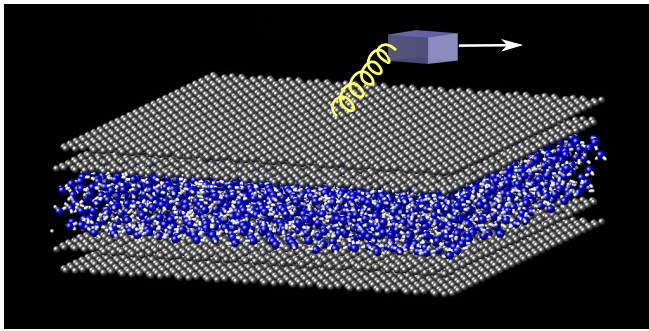


FIG. 1: A sketch of our simulation box. Carbon atoms are shown in grey, oxygen in blue, and hydrogen in white. The topmost and bottommost graphene sheets are rigid. The topmost sheet is attached with a spring to a support that moves at constant velocity during sliding runs.

II. DESCRIPTION OF THE SIMULATIONS

For reasons of computational power, it is impossible to simulate two realistic surfaces with a number of contact asperities. Even a single asperity moving at the velocities of an AFM experiment is not yet possible¹⁶. We therefore investigate a relatively small single asperity under a range of conditions that are likely to occur in a large sliding system.

We simulate various amounts of water molecules between two bi-layer graphene slabs as illustrated in Fig. 1 with a total of $4N_C$ atoms. The simulations were performed using the MD package LAMMPS¹⁷ with water described by the TIP4P/2005 model¹⁸ and the graphene sheets described using the AIREBO reactive force-field¹⁹. The interaction between water molecules and graphene is modeled with a Lennard-Jones potential between the oxygen and carbon atoms with parameters $\epsilon = 4.063$ meV, $\sigma = 0.319$ nm⁹. The carbon, oxygen, and hydrogen atoms are placed in a simulation box with periodic boundary conditions in x and y with sizes of 6.395 nm by 5.964 nm. In the z direction (orthogonal to the slab) the box is so large as to be effectively infinite (800 nm).

The outer carbon layers are kept internally rigid while the middle inner layers are mobile and internally fully flexible. The AIREBO potential, like most carbon potentials with long-range interactions based on Lennard-Jones²⁰, has a problem with underestimating the inter-layer corrugation. In order to prevent the mobile layers from slipping relative to their nearby rigid layers, especially during the sliding simulations, we add a spring between the centers of mass of each mobile layer and its nearest rigid layer. The spring constant is equal to 41 meV/Å² per atom, which was chosen so as to be consistent with experimentally determined inter-layer interactions for small displacements. The bottommost layer is kept at a fixed position while the topmost layer is coupled in the x and y directions with a spring (spring constant also 41 meV/Å² per atom) to a support that is kept at a fixed position during equilibration, and moves

at constant velocity during sliding. Pressure is applied through a uniformly distributed force on the topmost carbon layer. We also vary the amount of water in our simulation between $N_O/N_C = 0.16$ and 1.33, where we denote the total number of water molecules by N_O .

In a normal equilibrium simulation of a confined liquid, it would be the pressure that determines N_O , through a reservoir with a barostat. When the load on the contact is increased, the liquid flows out. However, in reality, when the surfaces are very large or rough, this squeezing out of the liquid can be hindered²¹. Thus, in a large moving contact, it is not a given that the system is in such equilibrium. For our purposes, there is therefore no direct link between the load/pressure and N_O , and these must be treated as independent parameters. While this means that in our simulations we must investigate a larger set of parameter combinations, we do not need to simulate a large liquid reservoir.

We employ Langevin dynamics for thermostating with damping constant chosen equal to 1 (ps)⁻¹. This damping coefficient is sufficiently small so as to not cause severe distortions of the dynamics even in the areas where it is applied²². The thermostat is always applied to all mobile carbon atoms and, whenever we do not slide the system, the water molecules are also thermostatted. In friction simulations, however, care should always be taken with thermostating, as this can severely distort results²². Whenever we subject the system to sliding, we therefore only thermostat the mobile carbon atoms.

Initial conditions are constructed by arranging the desired number of water molecules in a regular grid (but not an equilibrium structure) at approximately the density of water under ambient conditions. The carbon slabs are placed at initial positions far enough apart to contain the water molecules. We then simulate the system for some time under various load and temperature conditions as described below.

A. Equilibration procedures

Since we are interested in studying friction, which is a nonequilibrium process, we must investigate also how equilibrium can be reached. Specifically, a moving asperity leads to time-dependent load variations which can affect the structure of the confined material and we thus first investigate the equilibration of our system under two different sequences of conditions. In equilibration method one (temperature-scan method), we start immediately by applying high pressure, but also high temperature (2000 K), and then slowly reduce the temperature to 293 K over a time interval of 5 ns by ramping it down linearly. In equilibration method two (load-scan method), the system starts from room temperature, but the pressure is increased in steps at intervals of 50 ps to 0.01, 0.02, 0.1, nN/atom, and after that it is incremented by 0.1 nN/atom every 50 ps.

These two different equilibration methods give an in-

dication of what happens under different sliding conditions. At high sliding speeds, the pressure in the contact increases rapidly as the asperity approaches and the load-scan method produces the most representative conditions. At low sliding speeds, the confined water has ample time to equilibrate. The water in the contact is thus more likely to reach the global equilibrium, which is more easily reached in simulations by the temperature-scan method.

The temperature-scan method is known to reliably provide the equilibrium structure of bulk water at room temperature under high pressure, while the load-scan method does not. Specifically bulk ice VII is difficult to obtain in simulations by ramping up the pressure, but can be easily found by starting from high temperature and pressure and cooling the simulated system down slowly.

III. RESULTS

At low pressures/loads, the water remains liquid for both equilibration methods. At higher loads, however, the resulting structure depends on how the system approaches equilibrium.

We illustrate the different structures in Fig. 2. At high load, we find that the temperature-scan method produces a crystalline structure (Fig. 2a). The load-scan method on the other hand does not produce a crystalline structure, but rather something more reminiscent of the liquid structures at low load. Due to the high load, however, the arrangement of the water molecules follows somewhat the symmetry of the graphene sheets. In the context of MD simulations of water interacting with graphene, this is a crucial difference. MD simulations of this confined system^{8,10} so far have employed methods similar to the load-scan method. Thus it is not surprising that these simulations were not able to consistently reproduce the square/cubic structure of ice VII (or X) that has been seen in experiments⁴.

IV. CLASSIFICATION OF STRUCTURES

In order to better understand the different structures, we investigate the radial distribution function (RDF) and several other order parameters for a number of conditions. The RDFs are plotted in Fig. 3. Because of the confining geometry, the RDF is normalised not by $4\pi r^2 N/(L_x L_y L_z)$, but by $4\pi r^2 f(r, d) N/(L_x L_y d)$ with $f(r, d) = d/2r$ if $r > d$ and $f(r, d) = (1 - r/2d)$ if $r < d$. This is the RDF one would find for a slab of density $N/(L_x L_y d)$ and height d in the z direction. The height d was estimated from the maximum and minimum z coordinates of all oxygen atoms.

For the system that results from the temperature-scan approach, the RDFs at higher loads show the typical isolated peaks of a crystalline structure. Interestingly, at the lowest load of 0.1 nN/atom the RDF is very similar

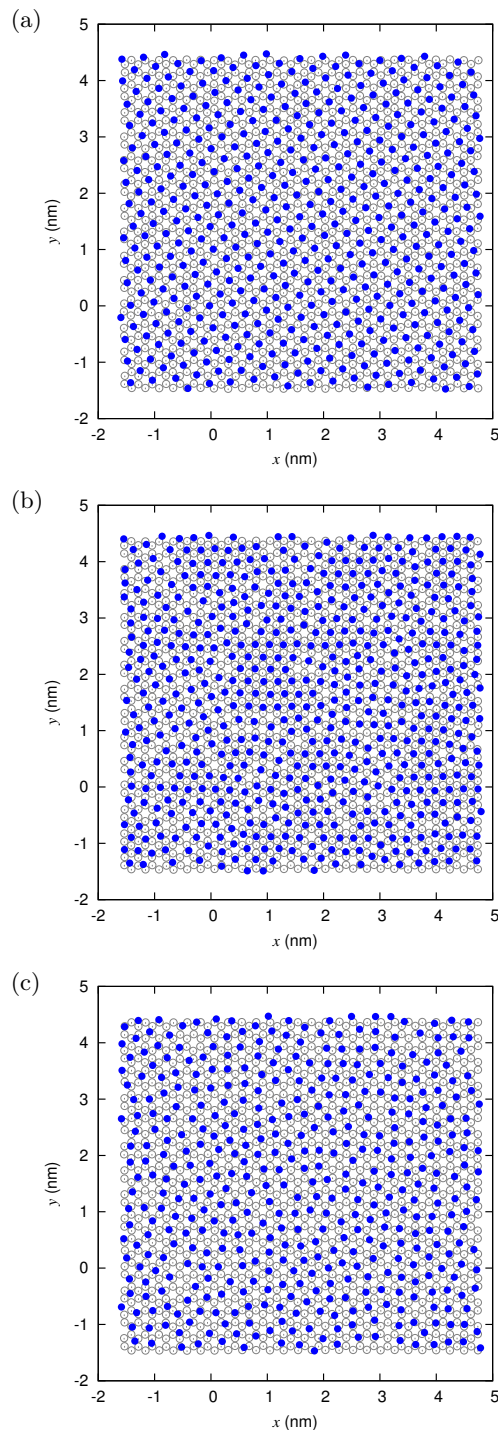


FIG. 2: The oxygens in the bottom layer of the water (filled symbols) together with the carbons in the top layer of the bottom graphene slab (open symbols) for three different cases: ice-like obtained by slowly reducing the temperature at high pressure (temperature-scan, top), liquid-like obtained by rapidly increasing the pressure at constant temperature (load-scan, middle) and liquid-like at lower pressure (bottom). At low loads the system equilibrates more easily. Ice-like structures appear at sufficiently high pressures, after careful equilibration, as expected from the phase diagram of bulk water. In these simulations $N_O/N_C = 1.33$ and the loads were (ramped up to) 1.0 nN/atom for (a) and (b), and 0.1 nN/atom for (c).

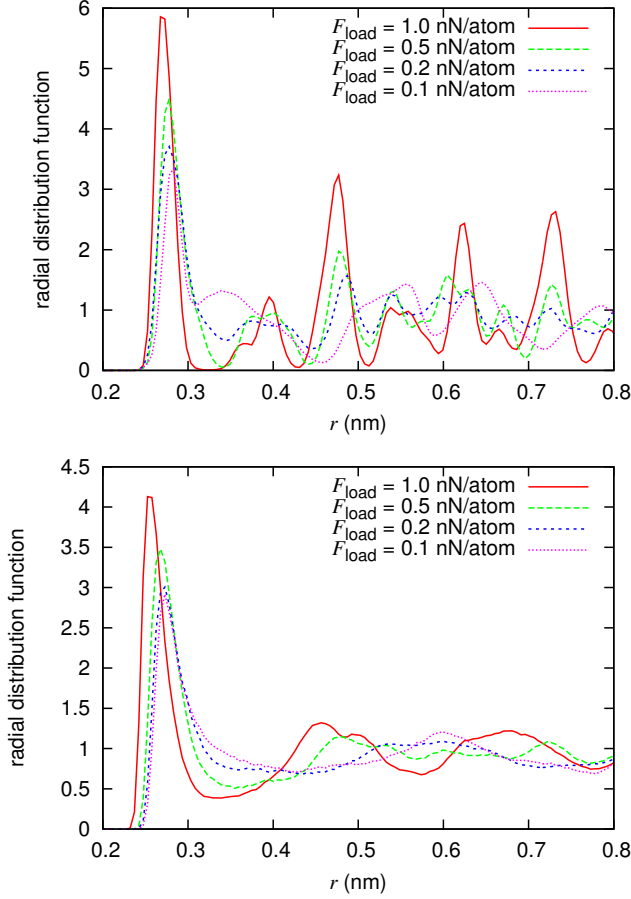


FIG. 3: Oxygen-oxygen radial distribution functions obtained from the temperature-scan method (top) and from the load-scan method (bottom). The temperature-scan method results in more ice-like structures with rather well-defined peaks in the RDF while the load-scan method results in significantly more disordered, liquid-like environments. In both these simulations $N_O/N_C = 1.33$.

to that found for the first layer of liquid TIP4P/2005 water on a BaF_2 substrate²³ with significant intensity at the interstitial distance around 0.35 nm and a near-complete loss of the second coordination shell around 0.45 nm. In ref.²³ this was interpreted as a high-density form which was fully consistent with the experimental x-ray absorption spectra. A difference between those results and ours is the presence here of significantly more structured peaks at intermediate distances.

Turning to the simulations with ramped-up load at constant temperature, we find much more smeared-out RDFs with structure consistent with a high-density liquid²⁴; only at the highest load do we find well-developed shell-structure, but still with peaks that are significantly broader than for the temperature scan simulations. Again, we find strong similarities between the present results and those of ref.²³ for the high-density liquid and NaCl solution. In both the latter cases there is enhanced intensity in the interstitial region, a near-

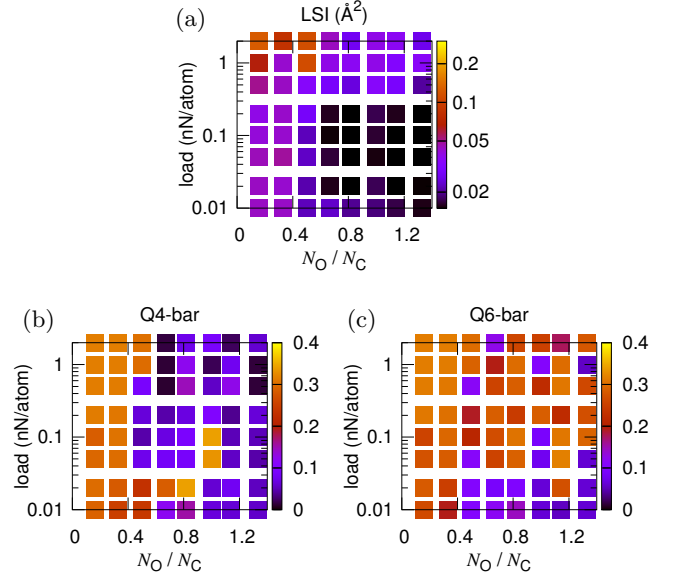


FIG. 4: Thickness-pressure plot of the average Local Structure Index (LSI), \bar{q}_4 , and \bar{q}_6 . For comparison, 1 nN/atom of load corresponds to a pressure of 38 GPa.

complete loss of the second shell and a build-up of intensity around 0.6 nm.

In Fig. 4 we classify the structure(s) in more detail through three order parameters as a function of the number of water molecules and the load, the Local Structure Index (LSI)^{25,26} and the local bond order parameters \bar{q}_4 and \bar{q}_6 ²⁷.

The LSI measures the degree of tetrahedral order versus disorder around a water molecule out to the second shell where the cutoff is set at 0.37 nm^{25,26}. It is defined as $I(i) = \frac{1}{n(i)} \sum_{j=1}^{n(i)} [\Delta(j;i) - \bar{\Delta}(i)]^2$ where $n(i)$ is the number of oxygen atoms out to the cutoff distance. These are ordered according to the distance from the central oxygen as $r_{i1} < r_{i2} < \dots < r_{in(i)}$, $\Delta(j;i) = r_{i,j+1} - r_{i,j}$ is the radial distance between the ordered oxygen neighbors and $\bar{\Delta}(i)$ is the mean of the sequential distances around the oxygen in molecule i . For a very structured tetrahedral environment there will be a large first distance followed by three very small distances and then a jump to the second shell. This situation will give a large squared deviation from the mean and thus a large LSI value while a more disordered local structure will give a low value.

We determine the symmetry of the phases using the local bond order parameters \bar{q}_4 and \bar{q}_6 ²⁷ applied to the oxygen atoms. These are based on the Steinhardt bond-order parameters²⁸, but are more sensitive to the local structure. They can be written as a local sum over spherical harmonics Y_{lm} of the relative positions between the

particles \vec{r}_{ij} as

$$\bar{q}_l(i) = \sqrt{\frac{4\pi}{2l+1} \sum_{m=-l}^{m=l} |\bar{q}_{lm}(i)|^2}, \quad (1)$$

$$\bar{q}_{lm}(u) = \frac{1}{N_b(i)+1} \sum_{k \in \text{nn} \cup i} q_{lm}(k), \quad (2)$$

$$q_{lm}(i) = \frac{1}{N_b(i)} \sum_{j \in \text{nn}} Y_{lm}(\vec{r}_{ij}), \quad (3)$$

where nn indicates the set of nearest neighbors of particle i and $N_b(i)$ is the number of nearest neighbors. Nearest neighbors are defined as particles within a specific distance from each other, in our case 0.37 nm. The quantities $\bar{q}_4(i)$ and $\bar{q}_6(i)$ are averaged over all oxygen atoms to obtain \bar{q}_4 and \bar{q}_6 respectively.

At low coverage, both \bar{q}_4 and \bar{q}_6 are high, as is the LSI. This indicates that there is crystalline structure in the system, but it is not consistent with a specific bulk symmetry. This is related to the fact that at low coverages there are only one or two layers of water molecules and the order parameters \bar{q}_4 and \bar{q}_6 are intended for use in bulk materials. The LSI plot shows low values for loads up to 0.2 nN/atom and coverage N_O/N_C above 0.6. This indicates strongly disordered local environments for this range of parameters. As expected, increasing the load leads to somewhat higher LSI values, *i.e.* slightly more order as the interaction with the graphene sheets is strengthened, with the highest values found for the highest loads at the lowest coverages. Closer visual inspection shows that the oxygen atoms in this regime are arranged in a single layer with inlayer structure. The distance between the oxygen atoms is approximately 0.27 nm and the atoms are arranged in a square grid. As the pressure increases, the structure adapts more to the graphite substrate, which distorts it from square to diamond-like.

At high loads and high coverage, the low LSI values indicate disorder, while the combination of high \bar{q}_6 and low \bar{q}_4 indicates an underlying BCC symmetry²⁷. We have confirmed this by visual inspection. The distance between the carbon atoms within one layer is approximately 0.39 nm. The single-layer structure with spacing 0.27 nm is likely the (0,1,1) face of this BCC structure.

V. DISCUSSION

Our results can be interpreted by comparing to the phase diagram of bulk water. The crystalline structure we observe for the temperature-scan method is consistent with bulk ice VII. At room temperature, water can freeze at pressures above of 0.9 GPa, forming tetragonal ice VI. Above about 2 GPa the stable phase is ice VII, which has a BCC arrangement of oxygen atoms²⁹. Above about 60 GPa, ice VII undergoes a continuous transition to ice X that is related to a rearrangement of the hydrogens. It is interesting to note that ice VII must be formed

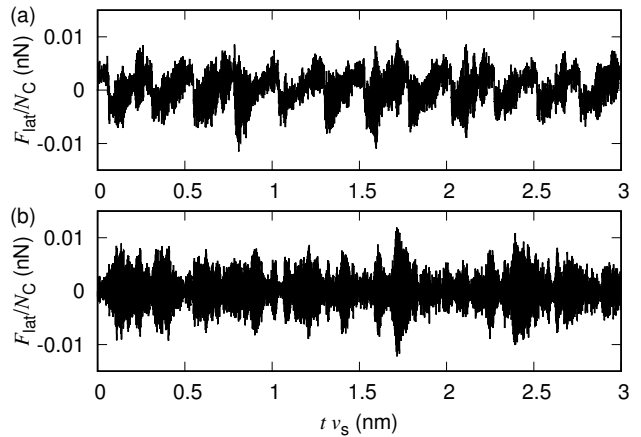


FIG. 5: Force traces for identical parameters (boundary layer thickness, sliding velocity, etc) but different initial conditions, liquid-like (a) and ice VII-like with free sliding (b). Due to the incommensurate lattice parameters of ice VII and graphite, there is superlubric sliding between the ice and graphite. The liquid-like water rearranges in a configuration that is strongly commensurate with the graphite, and thus has higher friction. The stick-slip period is consistent with the graphite substrate. In these simulations $N_O/N_C = 1.33$ and the load was (ramped up to) 0.5 nN/atom. The average lateral forces were 0.33 pN/atom for the liquid-like water and 0.03 pN/atom for the ice VII-like water.

by reducing the temperature of water at high pressures, rather than by increasing the pressure at ambient temperature.

Our simulations go up to significantly higher pressures than those of^{4,8–10}, all of which consider otherwise similar confining geometries. Moreover, these previous simulations did not vary the temperature during equilibration. This is likely why the confined ice VII structure that we find was not observed. The authors of Ref.⁸ already noted that at higher pressures they were not able to obtain convergence, consistent with our observations of the difference between the load and temperature scans. The transmission electron microscopy (TEM) experiments of Ref.⁴ were accompanied by simulations at pressures up to 1 GPa. Contrary to the TEM experiments, those simulations indicate an FCC-like lattice. Given the setup of the simulations, we believe that this FCC structure may have been related either to ice VI, or to the rhombic structure found at extremely low pressure in other simulations⁸. While the authors of Ref.⁸ did not evaluate this possibility explicitly, it appears that their TEM measurements would be consistent with square ice with a multi-layer BCC lattice.

We also briefly discuss squeezing out of the water. To investigate this we have performed simulations of a larger system, where the bottom sheets were 1.5 times larger in both directions, while the top sheets were kept at the same size. The water could thus escape from the contact asperity through the slit in the top sheet. We then slowly moved the plates together and recorded the force needed

to squeeze out the simulated water molecules into the vacuum above the top plate. The load needed to push out the last layer corresponds to about 0.1 nN/atom, which equates to approximately 4 GPa, too low for the formation of bulk ice VII. The extreme nonequilibrium nature of friction, and the long time scales associated with squeezing out of liquid, can lead to much higher pressures in real contacts.

VI. FRICTION AND COMPARISON TO AFM EXPERIMENTS

In general, interfaces between crystalline solids with nonmatching lattice parameters tend to have low friction if the crystals are sufficiently rigid³⁰. Ice VII and graphene constitute a combination with incommensurate lattice parameters and we have checked that this indeed leads to low friction. In Fig. 5 we show the lateral force as a function of time for two samples, one with liquid-like order, and one with ice VII-like. Due to the low-friction slide plane between the ice and carbon, the friction for the ice is lower. In the liquid-like system, there is a much stronger signature of stick-slip, with a period that is consistent with the lattice period of graphene.

In the experiments¹⁵ at high velocities the same stick-slip was observed that we see in our simulations of sliding with liquid-like confined water, i. e. with the lattice period of graphite. At high velocities we expect that the rapid increase in the pressure under the tip is best represented by the load-scan simulations, and thus we indeed expect liquid-like structure under those conditions.

At low velocities, the experiments¹⁵ show a high friction with a stick-slip period different from the lattice period of graphite. This lattice period is consistent with the period that we find for the crystalline ice structure that results from the temperature-scan equilibration method. We thus conclude that very probably ice VII is formed in these experiments.

In these experiments, however, its presence in the contact does not lead to superlubric sliding, but rather to high friction. This may be due to the difference in configuration between the experiments and our simulations. In the experiments, the possible slide planes are severely restricted. The graphite substrate in the experiments is probably (nearly) atomically flat over the distance that the tip travels, and the ice could, in principle, slide easily with respect to the surface. This could however be prevented because in order for the block of ice under the tip to slide, it would need to displace the liquid water surrounding it. The surface roughness of the tip also prevents the tip from sliding easily with respect to the ice. We suspect that as a result of this, in the experiments there is no clear slide plane as there is in the somewhat idealised solutions. Instead, the ice has to be fractured, and ice slides against ice with the same lattice constants, which produces high friction and a stick-slip period corresponding to ice, not graphite. When graphite is used as a solid lubricant, however, water is sandwiched between

flakes of (nearly) atomically flat graphite or graphene. With regard to which slide planes are possible, the situation in practice may be more similar to our simulations than to the experiments.

VII. CONCLUSIONS

The phase diagram of bulk water is already complicated, but in the present case, it appears that the extreme confinement of a few layers actually does not increase the level of complexity drastically. We find from our simulations that the experiments for water on graphite^{13,15} and graphene⁴ can be explained by considering the formation of ice VII. This ice phase is formed at extremely high pressures, but it is metastable under a wide range of conditions, including ambient³¹. In our simulations, its formation depends strongly on how the system is treated, which is consistent with the velocity-dependence found in experiments¹⁵. We also note that the presence of graphene or graphite likely contributes to the stability of ice VII: through the symmetry-breaking by the surface, and possibly also the electronic structure of the graphene⁹. Moreover, the similarities between our simulation results and measurements performed on water on a BaF₂ substrate²³ further support an interpretation based on the properties of water rather than those of the surface.

We have also investigated the effect of the presence of ice VII on the friction and find that it has the potential to drastically lower friction through the mechanism of structural superlubricity. Due to the difference in lattice parameters between the ice and graphite, the two slide easily with respect to each other. For this to happen in a real system, however, it would require atomically flat surfaces. In the AFM experiments^{13,15}), this sliding was prevented by the geometry of the contact. Nevertheless, in a solid lubricant, nearly atomically flat graphite and graphene flakes slide with respect to one-another, and it may be possible for graphene and ice to slide, thus reducing the friction. We therefore conclude that the presence of ice VII between layers of graphene or graphite can explain why graphite is much more effective as a solid lubricant in humid conditions than in dry conditions. Moreover, since the properties of the confined ice are clearly related to the bulk ice VII, its formation may not depend strongly on the surface used. It might thus be possible to cover other surfaces besides graphite with ice VII in order to reduce friction.

Acknowledgments

ASdW acknowledges support from the Swedish Research Council (Vetenskapsrådet), the COST action MP1303, and the Swedish National Infrastructure for Computing (SNIC).

- ¹ C. Donnet and A. Erdemir, *Tribol. Lett.* **17**, 389 (2004).
- ² A. S. de Wijn, A. Fasolino, A. E. Filippov, and M. Urbakh, *Europhysics Lett.* **95**, 66002 (2011).
- ³ D. Berman, S. A. Deshmukh, S. K. R. S. Sankaranarayanan¹, A. Erdemir, and A. V. Sumant, *Science* **348**, 1118 (2015).
- ⁴ O. Algara-Siller, G. and Lehtinen, F. C. Wang, R. R. Nair, U. Kaiser, H. A. Wu, A. K. Geim, and I. V. Grigorieva, *Nature* **519**, 443 (2015).
- ⁵ K. Xu, P. Cao, and J. R. Heath, *Science* **329**, 1188 (2010).
- ⁶ N. Severin, P. Lange, I. M. Sokolov, and J. P. Rabe, *Nano Lett.* **12**, 774 (2012).
- ⁷ A. Verdaguer, J. J. Segura, L. López-Mir, G. Sauthier, and J. Fraxedas, *J. Chem. Phys.* **138**, 121101 (2013).
- ⁸ H. Mosaddeghi, S. Alavi, M. H. Kowsari, and B. Najafi, *The Journal of Chemical Physics* **137**, 184703 (2012), URL <http://scitation.aip.org/content/aip/journal/jcp/137/18/10.1063/1.4763984>.
- ⁹ G. Cicero, J. C. Grossman, E. Schwegler, F. Gygi, and G. Galli, *Journal of the American Chemical Society* **130**, 1871 (2008).
- ¹⁰ S. Han, M. Y. Choi, P. Kumar, and H. E. Stanley, *Nature Physics* **6**, 685 (2010).
- ¹¹ S. Cervený, F. Mallamace, J. Swenson, M. Vogel, and L. Xu, *Chem. Rev.* (2016).
- ¹² K. Koga, G. T. Gao, H. Tanaka, and X. C. Zeng, *Nature* **412**, 802 (2001).
- ¹³ K. B. Jinesh and J. W. M. Frenken, *Phys. Rev. Lett.* **96**, 166103 (2006), URL <http://link.aps.org/doi/10.1103/PhysRevLett.96.166103>.
- ¹⁴ M. Dienwiebel, G. S. Verhoeven, N. Pradeep, J. W. M. Frenken, J. A. Heimberg, and H. W. Zandbergen, *Phys. Rev. Lett.* **92**, 126101 (2004).
- ¹⁵ K. B. Jinesh and J. W. M. Frenken, *Phys. Rev. Lett.* **101**, 036101 (2008), URL <http://link.aps.org/doi/10.1103/PhysRevLett.101.036101>.
- ¹⁶ Q. Li, Y. Dong, D. Perez, A. Martini, and R. W. Carpick, *Phys. Rev. Lett.* **106**, 126101 (2011), URL <http://link.aps.org/doi/10.1103/PhysRevLett.106.126101>.
- ¹⁷ S. J. Plimpton, *J. Comp. Phys.* **117**, 1 (1995), <http://lammps.sandia.gov>.
- ¹⁸ J. L. F. Abascal and C. Vega, *J. Chem. Phys.* **123**, 234505 (2005).
- ¹⁹ S. J. Stuart, A. B. Tutein, and J. A. Harrison, *The Journal of Chemical Physics* **112**, 6472 (2000), URL <http://scitation.aip.org/content/aip/journal/jcp/112/14/10.1063/1.481208>.
- ²⁰ M. Reguzzoni, A. Fasolino, E. Molinari, and M. C. Righi, *Phys. Rev. B* **86**, 245434 (2012), URL <http://link.aps.org/doi/10.1103/PhysRevB.86.245434>.
- ²¹ B. N. J. Persson, *Sliding Friction: Physical Principles and Applications* (Springer-Verlag Berlin, 2000).
- ²² M. M. van Wijk, A. S. de Wijn, and A. Fasolino, *Journal of Physics: Condensed Matter* **28**, 134007 (2016), URL <http://stacks.iop.org/0953-8984/28/i=13/a=134007>.
- ²³ S. Kaya, D. Schlesinger, S. Yamamoto, J. T. Newberg, H. Bluhm, H. Ogasawara, T. Kendelewicz, G. E. Brown Jr., L. G. M. Pettersson, and A. Nilsson, *Sci. Rep.* **3**, 1074 (2013).
- ²⁴ A. K. Soper and M. A. Ricci, *Phys. Rev. Lett.* **84**, 2881 (2000).
- ²⁵ E. Shiratani and M. Sasai, *J. Chem. Phys.* **104**, 7671 (1996).
- ²⁶ E. Shiratani and M. Sasai, *J. Chem. Phys.* **108**, 3264 (1998).
- ²⁷ W. Lechner and C. Dellago, *The Journal of Chemical Physics* **129**, 114707 (2008), URL <http://scitation.aip.org/content/aip/journal/jcp/129/11/10.1063/1.2977970>.
- ²⁸ P. J. Steinhardt, D. R. Nelson, and M. Ronchetti, *Phys. Rev. B* **28**, 784 (1983), URL <http://link.aps.org/doi/10.1103/PhysRevB.28.784>.
- ²⁹ B. Kamb and B. L. Davis, *Proc. Nat. Acad. Sci. USA* pp. 1433–1439 (1964).
- ³⁰ M. Peyrard and S. Aubry, *J. Phys. C* **16**, 1593 (1983).
- ³¹ S. Klotz, J. M. Besson, G. Hamel, R. J. Nemes, J. S. Loveday, and W. G. Marshall, *Nature* **398**, 681 (1999).